J Eng Math (2009) 64:207–218
DOI 10.1007/s10665-009-9282-2

Water distribution under trickle irrigation predicted using artificial neural networks

N. Lazarovitch · M. Poulton · A. Furman · A. W. Warrick

Received: 16 February 2009 / Accepted: 23 February 2009 / Published online: 25 March 2009

Abstract An artificial neural network (ANN) technology is presented as an alternative to physical-based modeling of subsurface water distribution from trickle emitters. Three options are explored to prepare input–output functional relations from a database created using a numerical model (HYDRUS-2D). From the database the feasibility and advantages of the three alternative options are evaluated: water-content at defined coordinates, moment analysis describing the shape of the plume, and coordinates of individual water-content contours. The best option is determined in a way by the application objectives, but results suggest that prediction using moment analyses is probably the most versatile and robust and gives an adequate picture of the subsurface distribution. Of the other two options, the direct determination of the individual water contours was subjectively judged to be more successful than predicting the water content at given coordinates, at least in terms of describing the subsurface distribution. The results can be used to estimate subsurface water distribution for essentially any soil properties, initial conditions or flow rates for trickle sources.

Keywords Artificial neural networks · Drip irrigation · Spatial moments · Water flow

1 Introduction

Designs of drip irrigation systems involve selection of an optimal combination of emitter discharge rate and spacing between emitters for a given set of soil, crop and climatic conditions, as well as understanding the wetted-zone

N. Lazarovitch (✉)
The Wyler Department of Dryland Agriculture, French Associates Institute for Agriculture and Biotechnology of Drylands, Jacob Blaustein Institutes for Desert Research, Ben-Gurion University of the Negev, Sede Boqer Campus, Midreshet Ben-Gurion 84990, Israel
e-mail: lazarovi@bgu.ac.il

M. Poulton
Mining and Geological Engineering, University of Arizona, Tucson, USA

A. Furman
Civil and Environmental Engineering, Technion-Israel institute of Technology, Haifa 32000, Israel

A. W. Warrick
Soil Water and Environmental Science, University of Arizona, Tucson, USA

pattern around the emitter [1,2]. Water distribution is affected by many factors including soil hydraulic characteristics, initial conditions, emitter discharge rate, application frequency, evaporation, transpiration and the root-system architecture.

Mathematical models can be used to increase the ability to predict water, fertilizer and salt movement and distribution in the soil [3]. In practice, the actual application of such models depends on the capability to perform this analysis and optimization for relevant cases with reasonable effort. Both analytical and numerical models are used to predict water distribution under drip irrigation [4–6]. While transient analytical models are generally restricted to the Green–Ampt model [7] or to the use of Gardner's [8] hydraulic conductivity function, numerical models are more flexible and can implement practically any model for the soil hydraulic properties. Complex systems including irregular boundaries and non-constant boundaries and initial conditions are also amenable to analysis. On the other hand, computations with analytical models are much less tedious than numerical solutions and water distributions can easily be computed independently for any time considered without running a full simulation. This is a strong advantage when massive amounts of calculations are required such as for sensitivity analyses [9]. Another limitation of numerical models is associated with the typical need to discretize time and space. Inappropriate discretization can lead to bias in the solution. Although the learning procedures for the time discretization for adjusting the time step of the numerical solution are widely used, the adaptive-grid procedures for the space discretization are rarely used [10].

Artificial neural networks (ANN) are a robust pattern recognition technique that can be used for relating system inputs and outputs when the physical relationships describing the system are very complex. ANN creates a map between measured system inputs and outputs. Provided that the measured data adequately describe, sample, and bound the system, the neural network will find a set of weights that map input to output data with minimum error. ANN models are widely used for prediction of soil hydraulic properties [e.g., 11–14]. The assumption is that soil–water retention and unsaturated hydraulic-conductivity curves can be determined from basic soil properties such as texture, bulk density or clay content. Combined with a user-friendly interface like `ROSETTA` [15] or `NEUROTHETA` [14] the ANN enable broad use of the hydraulic properties when the more tedious methods of direct measurement is impractical or not critical.

Further applications of ANN in soil science are limited and mostly associated with prediction of water flow and solute transport from laboratory, field or numerical experiments. Specifically, Schmitz et al. [16] proposed to use ANN for solving water flow from a surface point source. They used a physically based numerical subsurface flow model and ANN for solving the problem in two, fully separate steps. The first step utilizes the numerical model for calculating a large number of wetting profiles from various boundary and initial conditions. The resulting database of subsequent input/output values was used for training the ANN. In the second step, the fully trained ANN was used to estimate the location of the wetting fronts. In another study, Jiusheng et al. [17] used laboratory experiments to train the ANN in order to estimate nitrate concentration in the soil when the solution was applied from a surface point source. They conclude that the trained ANN model was reasonably accurate and using ANN can overcome the highly nonlinear complexity of the flow system.

Inspired by Schmitz et al. [16], we explore three different options to predict the water distribution in the subsurface. These represent different ways of approaching the problem of interest (the water distribution) and, at the outset, it is not known which method will give the most adequate information or even whether reasonable results can be attained. By developing the database using numerical models, the source of training data is limited only by computation resources, but if we choose all the temporal and spatial data from several scenarios, the results quickly form a huge database. Eventually, the database may be non-realistic when training an ANN. In order to develop our primary objective of predicting water distribution in the subsurface for drip irrigation, it is necessary to examine the alternative schemes, judge the effectiveness of each, and utilize databases of reasonable size. Concurrently, we evaluate feasibility and advantages of these options. If successful, the results from the trained system can be used to evaluate subsurface water patterns for any chosen soil, emitter flow rate or initial condition as a function of time without further numerical analyses.

2 Materials and methods

2.1 Subsurface flow model

Numerical solutions of Richards' [18] equation were implemented using the HYDRUS-2D code [19]. This code has been previously used to successfully simulate water flow from drip irrigation systems [6,20]. Surface point sources are considered resulting in three-dimensional axial-symmetry planes. The governing flow equation for three-dimensional isothermal Darcian flow in a variably saturated isotropic rigid porous medium presented by the mixed form of the Richards [18] equation:

$$\frac{\partial \theta}{\partial t} = \frac{1}{r}\frac{\partial}{\partial r}\left(rK\frac{\partial \psi}{\partial r}\right) + \frac{\partial}{\partial z}\left(K\frac{\partial \psi}{\partial z}\right) - \frac{\partial K}{\partial z}, \tag{1}$$

where θ is the volumetric water content [$L^3\,L^{-3}$], ψ is the soil matric head [L], K is the hydraulic conductivity [LT^{-1}], r and z are spatial coordinates [L] in the radial and vertical directions, respectively (z positive downward) and t is time [T]. In this study we are considering only the irrigation event, neglecting other processes occurring after the water is added (e.g., redistribution, water uptake, evaporation). A specialized version of the HYDRUS-2D code, a finite-element numerical code that solves the two-dimensional Richards equation, allows the spatial distribution of the source discharge rate at the soil surface to change with time [21,22]. This is done by switching from a Neumann (flux) to a Dirichlet (head) boundary condition if the surface pressure head required to accommodate the specified flux for a surface node is larger than 0. A sufficient number of surface nodes are switched in an iterative way until the entire irrigation flux is accounted for and the pond width is determined. Since the infiltration flux into the dry soil is larger for early times, the pond width continuously increases as irrigation proceeds. Other initial and boundary conditions for numerically solving [1] are

$$\psi(r, z, 0) = \psi_i, \tag{2}$$

$$\frac{\partial H}{\partial z} = \frac{\partial(\psi + z)}{\partial z} = 0, \quad r_0 < r < R, \quad z = 0, \tag{3}$$

$$\psi(r, z, t) = \psi_i, \quad r^2 + z^2 \to \infty, \tag{4}$$

$$\frac{\partial \psi}{\partial z} = 0, \quad z = Z, \tag{5}$$

where r_0 is the ponded radius [L], $H$is the total head [L], ψ_i is the initial soil matric head [L] and R and Z are the domain radius and depth [L], respectively.

The Mualem–van Genuchten soil hydraulic model [23,24] was selected for the numerical simulations:

$$S_e = \frac{\theta - \theta_r}{\theta_s - \theta_r} = \left[1 - |\alpha\psi|^n\right]^{-m}, \quad m = 1 - \frac{1}{n}, \tag{6}$$

$$K = K_S S_e^{0.5}\left\{1 - \left[1 - S_e^{1/m}\right]^m\right\}^2, \tag{7}$$

where S_e is the effective fluid saturation [–], θ_r and θ_s denote the residual and saturated water contents [$L^3\,L^{-3}$], respectively, K_s the saturated hydraulic conductivity [LT^{-1}] and α [L^{-1}], n [–], and m [–] are empirical shape parameters.

A flow domain was selected with $R = 1$ m and $Z = 2$ m. The flow domain was discretized into 1,123 nodes with significantly greater detail around the source (automated discretization by HYDRUS-2D default mesh generation parameters). Five homogenous soils with contrasting texture used in the simulations in order to have a representative matrix of variables that will allow comprehensive evaluation (The complexity of heterogeneous soil properties is beyond the scope of this paper) .The hydraulic properties of these soils are taken from [25] and summarized in Table 1. Five discharge rates, Q [$L^3\,T^{-1}$] were used: 0.0005, 0.001, 0.002, 0.005 and 0.008 $m^3\,h^{-1}$. Three initial effective fluid saturations, S_{ei} [–], were used: 0.01, 0.05 and 0.1. The total applied volume was 0.04 m^3 in all the simulations. Thus, simulated application duration varied between 80 h for $Q = 0.0005\,m^3\,h^{-1}$ and 5 h for

Table 1 Hydraulic properties for the 5 contrasting soils and the 4 test cases

Soil	θ_r	θ_s	α (m^{-1})	n	K_s ($m\,hr^{-1}$)
Sand	0.045	0.43	14.5	2.68	0.297
Loamy sand	0.057	0.41	12.4	2.28	0.146
Sandy loam	0.065	0.41	7.5	1.89	0.0442
Loam	0.078	0.43	3.6	1.56	0.0104
Silt loam	0.067	0.45	2.0	1.41	0.0045
Test Case 1	0.062	0.43	13.4	2.43	0.2
Test Case 2	0.062	0.43	10.7	2.13	0.1
Test Case 3	0.062	0.43	14.5	2.68	0.2
Test Case 4	0.062	0.43	10.6	2.13	0.2

$Q = 0.008\,m^3\,h^{-1}$. In all the simulations outputs were saved at 20 evenly spaced times. The result from all simulations is a dataset of 1,684,500 (5 soils × 5 discharge rates × 3 initial conditions × 1,123 nodes × 20 print times) vectors where each vector had eleven elements, θ_r, θ_s, α, n, K_s, Q, S_{ei}, t, r, z, θ.

2.2 Data gathering

In this section we will explore alternatives for decreasing the size of the database to a meaningful and reasonable size while remaining effective.

2.2.1 Method 1

This method consists of a coarse vector sampling from the total available vectors. The numbers of connection weights in the ANN have to be balanced against the available data with a general guideline of 4–10 times more training patterns than connection weights [26, p. 56]. Since we have 1,500 available water-content distribution snapshots (5 soils × 5 discharge rates × 3 initial conditions × 20 print times) we selected one to three random vectors that contain 11 elements (θ_r, θ_s, α, n, K_s, Q, S_{ei}, t, r, z, θ) from each snapshot. As mentioned, the simulations were conducted with a flow domain that has significantly greater detail around the source. To equalize the likelihood of each vector to be selected, HYDRUS-2D results were regridded to 1 × 1 cm grid where the grid points assumed to be that of the closest finite-element node using a separate program. The gridding procedure was accurate and reproduced 99.99% of the mass. One to three grid nodes were randomly selected from each of the 1,500 available snapshots. Care was taken that values were chosen only from locations that were greater than the initial value (with threshold of 0.001 for the reduced water content). This procedure yielded datasets of 1,500, 3,000 and 4,500 vectors with 11 elements including 10 inputs (θ_r, θ_s, α, n, K_s, Q, S_{ei}, t, r, z) and one output (S_e). The first 1,500 vectors are referred as Dataset 1 in Table 2; the 3,000 vectors as Dataset 2 in Table 2; and the entire 4,500 vectors as Dataset 3, also in Table 2.

2.2.2 Method 2

The second method utilizes spatial moments to represent water dynamics under drip irrigation [22]. This method allows a straightforward, physically meaningful description of the general pattern of water distribution around the surface. As opposed to traditional methods that require detailed information of the water-content distribution, moment analyses can accurately describe the water-content distribution in a statistical manner with just three numbers: the center of the added water (plume), z_C, and the spread of the plume about its center in the z- and r-directions, σ_z and σ_r. These three numbers define a spheroid about the center of the plume of added water. Any fraction of water added can be related to a "probability" curve relating the size of the spheroids which contains that amount of water.

Table 2 Fitting parameters R^2 and MSE

Method	Prediction values	R^2 training	R^2 testing	MSE
1	Dataset 1	0.9870	0.9858	0.0035
1	Dataset 2	0.9941	0.9894	0.0015
1	Dataset 3	0.9946	0.9922	0.0014
2	z_C	1.0000	0.9999	0.0137
2	σ_r	0.9999	0.9999	0.0023
2	σ_z	0.9999	0.9999	0.0047
3	$z_{\max}$, $S_{ec} = 0.15$	0.9935	0.9945	0.568
3	r_1, $S_{ec} = 0.15$	0.9937	0.9943	0.2497
3	r_2, $S_{ec} = 0.15$	0.9930	0.9924	0.179
3	r_3, $S_{ec} = 0.15$	0.9929	0.9905	0.215
3	r_4, $S_{ec} = 0.15$	0.9604	0.9458	2.353
3	$z_{\max}$, $S_{ec} = 0.5$	0.9941	0.9917	1.611
3	r_1, $S_{ec} = 0.5$	0.9970	0.9974	0.372
3	r_2, $S_{ec} = 0.5$	0.9970	0.9972	0.317
3	r_3, $S_{ec} = 0.5$	0.9960	0.9962	0.346
3	r_4, $S_{ec} = 0.5$	0.9668	0.9640	2.499
3	$z_{\max}$, $S_{ec} = 0.95$	0.9954	0.9956	0.257
3	r_1, $S_{ec} = 0.95$	0.9988	0.9990	0.314
3	r_2, $S_{ec} = 0.95$	0.9988	0.9991	0.285
3	r_3, $S_{ec} = 0.95$	0.9987	0.9986	0.316
3	r_4, $S_{ec} = 0.95$	0.9678	0.9791	2.766

A separate program was used to compute the moments directly from the HYDRUS-2D output. For expediency, an equally spaced grid was defined (1×1 cm) and values of water content in the grid points were assumed to be that of the closest finite-element node. The moments were then computed using the gridded values. More details for moment calculations can be found at [22]. This procedure yielded dataset of 1,500 vectors with 11 elements including 8 inputs (θ_r, θ_s, α, n, K_s, Q, S_{ei}, t) and 3 outputs (z_C, σ_r, σ_z).

2.2.3 Method 3

The third method uses coordinates of water-content contours directly. A separate program is used to locate these coordinates for each snapshot and contour of specific water content. First a contour of specific effective fluid saturation, S_{ec}, is selected and then the program finds the coordinates of the contour. The contours coordinates are defined using five r- and z-locations [(0, $z_{\max}$) (r_1, 0) (r_2, 0.15 $z_{\max}$) (r_3, 0.3 $z_{\max}$) (r_4, 0.9 $z_{\max}$)]. The $z_{\max}$ is the maximum depth of the effective fluid saturation contour and $r_1 - r_4$ are radial coordinates. The number of points to describe a curve is a compromise between detail and practicality of inputs. This procedure yielded a dataset of 1,500 vectors with 13 elements including 8 inputs (θ_r, θ_s, α, n, K_s, Q, S_{ei}, t) and 5 outputs ($z_{\max}$, r_1, r_2, r_3, r_4) for each S_{ec}. In this work S_{ec} was chosen to be 0.15, 0.5 or 0.9.

2.3 Neural network calculations

The nomenclature for artificial neural networks describes the architecture of the network in terms of the arrangement and connection between computing nodes and layers and the learning algorithm used to calculate the connection weights. We used one of the most common architectures, a multi-layer perceptron (MLP). The MLP consists of an input layer with a node or processing element (PE) for each element of the input pattern vector. The input PEs are connected to PEs in the next layer, the hidden layer, by weights that start with random values. Each PE in the hidden layer computes a weighted sum of the input data and the connection weights and passes that sum through an activation function. We used a hyperbolic tangent function for all of our networks. The output of the activation

function becomes the input to the next layer which is either another hidden layer or the output layer and the computations previously described are again applied. Once the signal reaches the output layer, the ANN-calculated output is compared to the desired output provided in the training set. Since the connection weights started with random values, there will be an error in the network output. This error is usually computed as a mean-squared error. The learning algorithm used determines how the connection weights are changed to compensate for the error. We used one of the most common learning algorithms, backpropagation, and a more sophisticated algorithm called the quasi-Newton method. Both algorithms were used in conjunction with each other. Backpropagation was used for the first 50 epochs of training (1 epoch = 1 complete pass through the training set) and then the quasi-Newton method was applied using the weights from backpropagation as the initial weights. The backpropagation algorithm is described in many publications including [26, p. 28] and will not be described in detail in this paper. The backpropagation algorithm uses a gradient-descent technique to find a set of connection weights that will provide a minimum error for all patterns in the training set. This algorithm is fast and often provides results that are good enough. Gradient descent, however, can be slow to converge to a minimum and can often get stuck in local minima on the error surface. More sophisticated methods to find a set of connection weights that will represent the global minimum of the error surface are conjugate gradient, Newton's method, quasi-Newton method, and Levenberg–Marquardt method.

The quasi-Newton method approximates the Hessian matrix rather than doing an exact calculation of the matrix and its inverse. The quasi-Newton method converges to the global minimum quickly but does have large memory requirements and sometimes cannot be used for large networks [26, p. 72], [27, p. 127], [28, p. 287].

The sizes of the input and output layers were fixed by the variables needed for each of the three methods we used to compute water content. The hidden layer size was computed iteratively by STATISTICA ANN software [29] to provide a minimum training error. For Method 1 we used two hidden layers each with 21 processing elements. For Method 2 we used two hidden layers each with 20 processing elements. For Method 3 we used two hidden layers each with 31 processing elements. The network architectures found to be optimal for each method are larger than typically expected but are a function of the complexity of the problem. Each network began training with the backpropagation algorithm for approximately 50 passes through the training set and then the quasi-Newton method was applied for 200–300 passes through the training set. Three partitions of the dataset are used for training, testing, and validation. 50% of the data are selected for training, 25% for validation, and 25% for testing. Testing is a blind test at the end of training and these data are not used for any aspect of network training. The validation set is used during training to determine if overtraining is taking place. The training process is stopped periodically and the weights frozen. The validation data are applied to the network and the errors calculated. Since the error on the training data will continue to decrease, we detect overtraining when the error on the validation data begins to increase. At that point, training is stopped, the weights frozen, and the test data are applied in a blind test.

3 Results and discussion

Training of a neural network was completed for each of the 3 different datasets in Method 1. Predicted effective fluid saturations, S_e, with the trained ANN as a function of the numerical model results are presented in Fig. 1 for Datasets 1 (1,500 points), 2 (3,000 points), and 3 (4,500 points). The R^2 and MSE for all methods and datasets are summarized in Table 2. Going from small to intermediate size of datasets for training increases the coefficient of correlation for testing (R^2) from 0.9858 to 0.9894. Increasing the size further for Dataset 3 made a smaller change in comparison to Dataset 2 ($R^2 = 0.9921$). Increasing the size of dataset decreased the mean squared error (MSE) from 0.0035 in Dataset 1 to 0.0014 in Dataset 2. A further increase of input data to 4,500 points did not make a great difference with respect to MSE (0.0014). The larger dataset concealed the extreme points (the points farthest from the 1:1 line) that appear in Fig. 1a and bunched most of the points in Fig. 1b and c.

With respect to Method 2, ANN predictions as a function of the numerical model results for center of the added water, z_C is depicted in Fig. 2a. The spread of the plume about its center in the r- and z-directions, σ_r and σ_z are presented in Fig. 2b and c, respectively. The ANN captured accurately the behavior with very small MSE and R^2 near 1 and the points tightly on the 1:1 line.

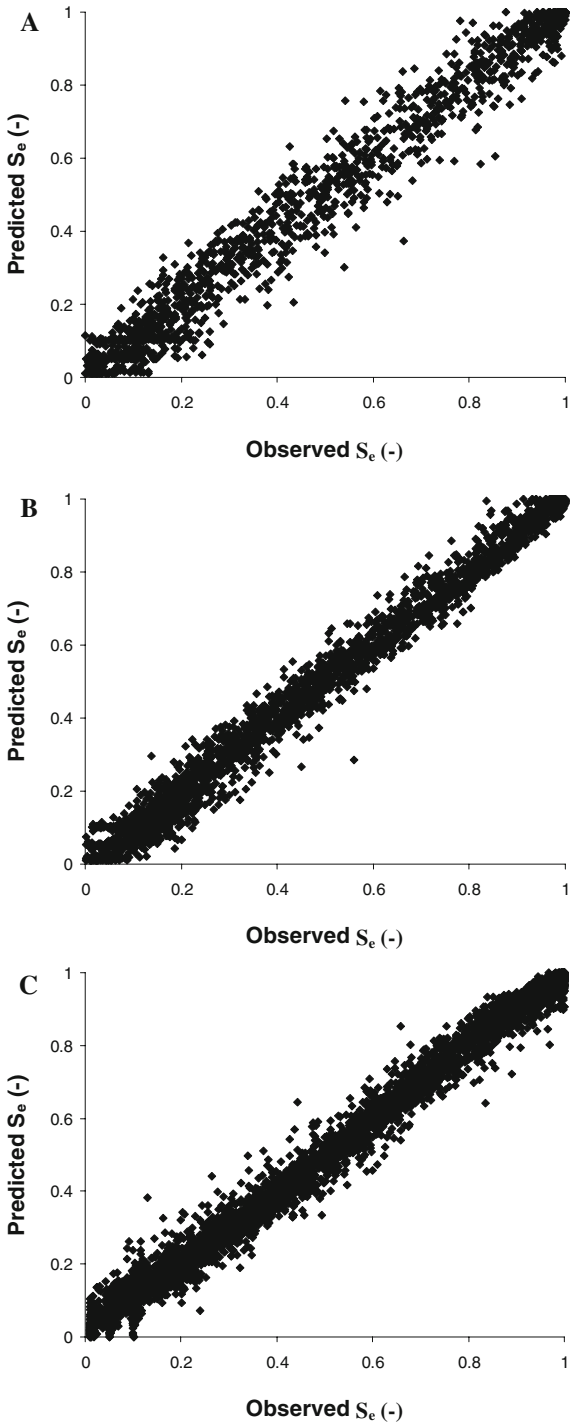

Fig. 1 Effective fluid saturation, S_e, with the ANN as a function of the numerical model results for: **a** Dataset 1; **b** Dataset 2; and **c** Dataset 3

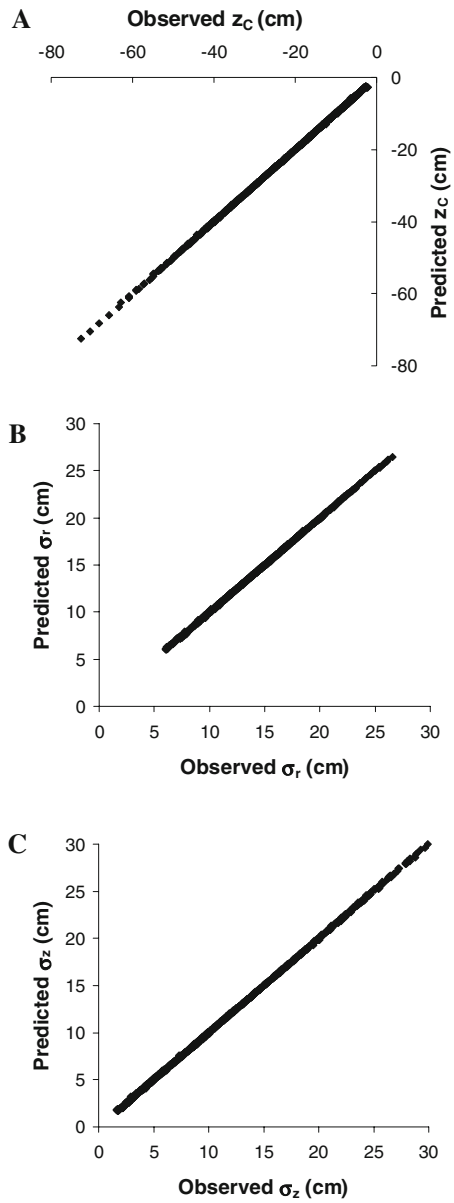

Fig. 2 ANN prediction as a function of the numerical model results for: **a** center of the added water (plume), z_C; **b** the spread of the plume about its center in the r-direction σ_r; and **c** the spread of the plume about its center in the z-direction σ_z

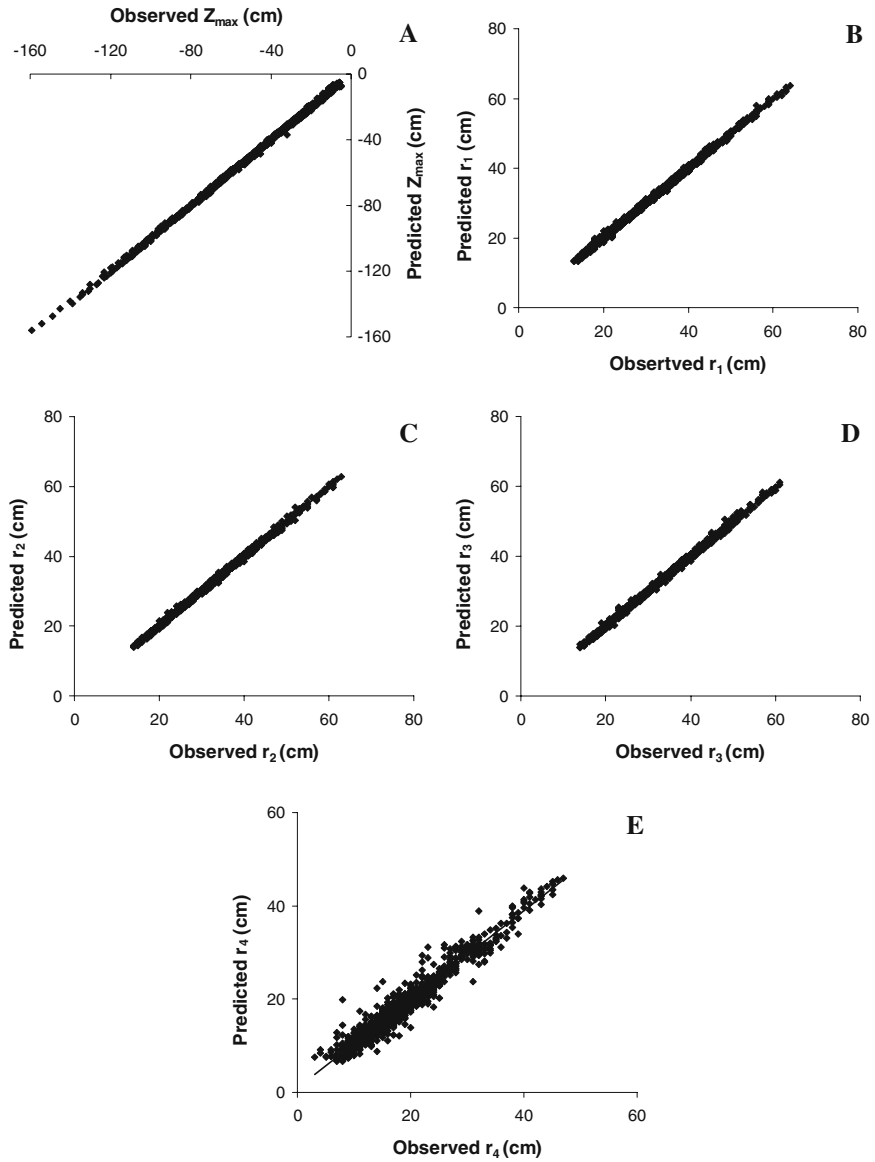

Fig. 3 ANN prediction as a function of the numerical model results for: **a** the maximum depth of the water-content contour, $\theta_c = 0.15$; **b** the radial coordinate, r_1, of the water-content contour; **c** the radial coordinate, r_2, of the water-content contour; **d** the radial coordinate, r_3, of the water-content contour; and **e** The radial coordinate, r_4, of the water-content contour

Finally, ANN predictions for Method 3 are plotted vs. the observed values for the effective fluid saturation contour, $S_{ec} = 0.15$ in Fig. 3. Figure 3a is for the maximum depth of the water-content contour, $z_{\max}$, 3b for the radial coordinate, r_1, 3c for the radial coordinate, r_2, 3d for the radial coordinate, r_3 and 3e for the radial coordinate, r_4. The predicted values are reasonable as confirmed again by small MSE and R^2 values near 1 as given in Table 2. Values of r_4 are predicted somewhat more poorly than $r_1$as can be viewed in the scatter diagram (Fig. 3e) as well as a smaller value R^2 and a larger MSE. These tend to correspond to positions deeper in the soil profile and are near the front of the added water. The statistics MSE and R^2 are given for other relative water contents $S_{ec} = 0.5$ and 0.95 are also included in Table 2 (but not as the scatter plots). These follow the same general trends as for $S_{ec} = 0.15$, with similar MSE and R^2 values and with the poorest fits for r_4.

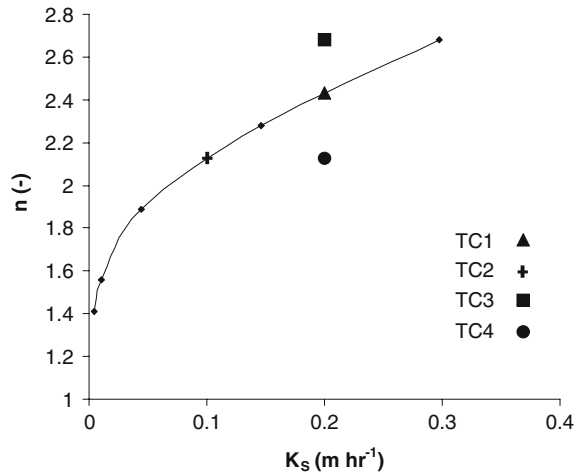

Fig. 4 Soil parameter n from [6] as a function of K_s for the four test cases

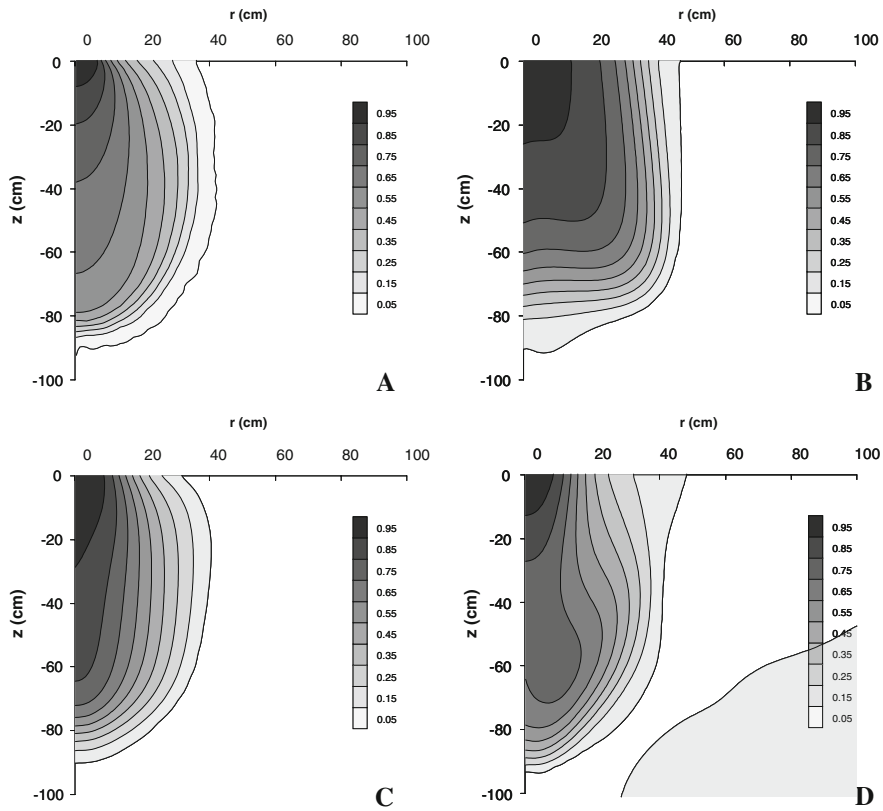

Fig. 5 Comparison of water-content profiles for Test Case 1 between **a** HYDRUS-2D results; **b** the first ANN method with Dataset 1; **c** the first ANN method with Dataset 2; and **d** the first ANN method with Dataset 3

After training was completed, testing data were obtained using 4 new simulations with different soil properties, initial conditions and discharge rate than used for the training sets. This provided subsurface water distribution to the end of 0.04 m^3 application. The values of the soil hydraulic properties for the test cases are summarized in Table 1. In all 4 test cases the discharge rate and the initial effective fluid saturation were 0.004 $m^3\,h^{-1}$ and 0.05, respectively. Soil parameter n from [6] as a function of K_s for the four test cases is showed in Fig. 4. The values of

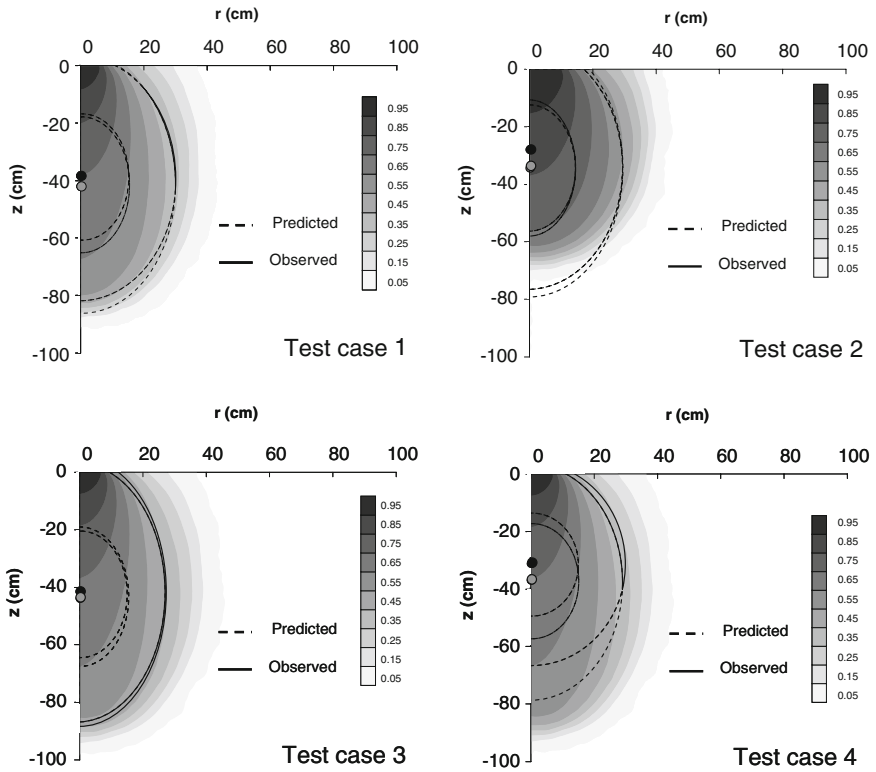

Fig. 6 Comparison of spheroids resulting moments calculations for all four test cases between HYDRUS-2D and ANN results from the second method

n and K_s for the 5 contrasting soils of Table 2 tend to fall on a single curve as demonstrated in Fig. 4. Test Cases 1 and 2 were chosen along this same curve and Test Cases 3 and 4 were deliberately chosen off the curve as shown.

The observed water-content distribution of the numerical simulation for Test Case 1 is depicted in Fig. 5a. The predicted water-content distributions for the three different nets that were trained using Datasets 1–3 are presented in Fig. 5b–d, respectively. Immediately, we observe that the original and predicted values in the regions closest to the source tend to be reasonably matched (that is by comparing the shaded regions of Fig. 5b–d to Fig. 5a). However, further from the source the adequacy of the results is questionable, especially for Fig. 5b and d. A somewhat surprising result, is that the "best" results overall are clearly for the training Sets 2 (as shown in Fig. 5c). This suggests that there is an optimum training set size and that over fitting can be undesirable in the case of the largest training set which results in Fig. 5d.

Comparisons of spheroids resulting from moments calculations for all four test cases are shown in Fig. 6. The "shading" is the HYDRUS-2D results for the water distribution, the solid curve is the observed ellipsoids and the shaded curve the predicted values. The given ellipsoids denote 1 and 2 "standard deviations" based on $k\sigma_r$ and $k\sigma_z$ with k equal to 1 for the inner ellipse or 2 for the outer. The inner contours define a region containing about 19% of the added water; the outer contours define a region containing about 72% of the added water. Also shown are the center of mass and the predicted center of mass. Although the general shape of the ellipsoids is captured in all four test cases, Test Case 4 tends to show the poorest comparison.

Comparisons of water-content contours $S_{ec} = 0.15$, 0.5 and 0.9 between HYDRUS-2D and ANN results from the third method for all test cases is presented in Fig. 7. The overall contours are reasonable except for Test Case 2 which shows a crossing over the 0.5 and 0.9 curves at about the 60 cm depth. This is due to an inadequate estimate for the $z_{\max}$ values. The general conclusion is that the results are best for Test Cases 1 and 4 and worse for Test Cases 2 and 3.

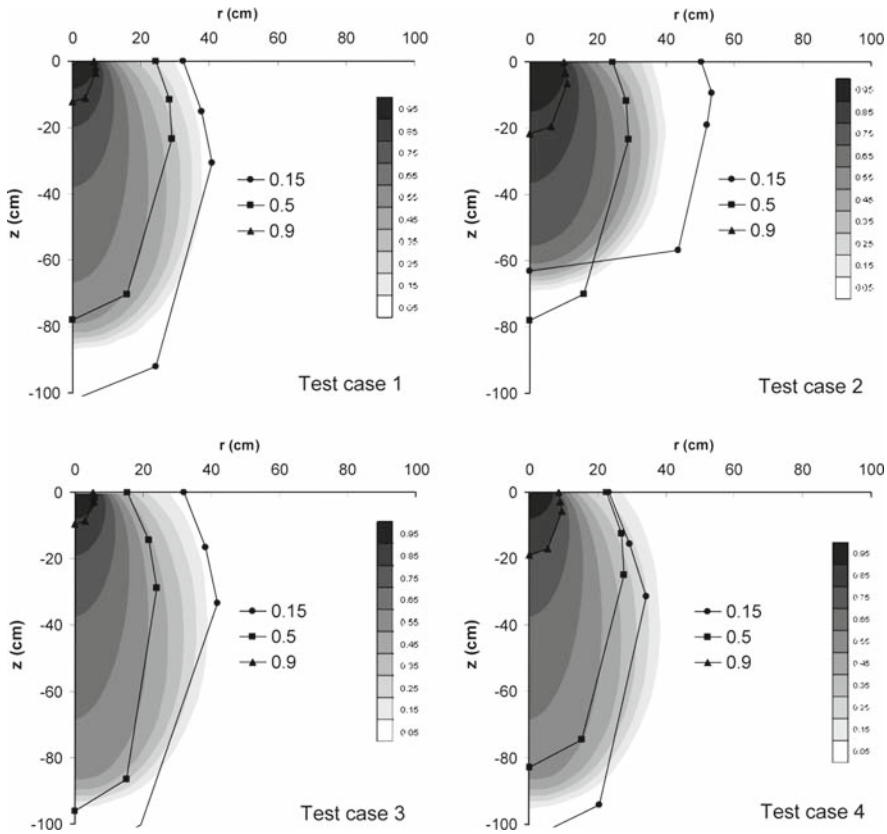

Fig. 7 Comparison of water-content contours, $S_{ec} = 0.15$, 0.5 and 0.9, between HYDRUS-2D and ANN results from the third method

4 Conclusions

This work encapsulates numerical modeling of complex systems into an easy to use form. The results are, for the most part, acceptable and allow the user to get an answer for any given time, soil hydraulic properties, initial and boundary conditions without having to perform a detailed numerical simulation. But at the same time, the results at times were disappointing, especially when the hydraulic properties tended to be dissimilar from those of the training set.

Three methods for describing subsurface water distribution were defined and tested. Method 1 which relied on predicting water contents for specified coordinates is probably the most obvious choice to use in terms of defining subsurface water. However, it appears to be the most difficult of the three methods and was sensitive to the training set used. Method 2 based on moment analyses is much less obvious, but appears to be the most robust of the three methods. The results sought in this case are not the distribution of the water contents but a center of mass and ellipsoidal contours which define where the added water resides in the profile. The ellipses (actually ellipsoids in 3-dimensions) shown correspond to approximate 19% and 72% of the added water, but others are possible using the same moments. Method 3 predicts a specified number of points for specific water contours (we chose five points for each contour). The results are best for the positions close to the source and tend to be more difficult to define in the lower portions of the profile near the maximum depths for which the water contents change.

In the future, we expect to use the trained dataset to predict water contents for a trickle source in a user-friendly environment by specifying only the input parameters with the results being computed essentially instantaneously using a spreadsheet environment. However, the potential applications are much broader with one intriguing application being to address the inverse problem of using measurements of moments based on a limited number of

observations and calculating soil hydraulic properties. The procedure also appears viable for other irrigation systems such as from surface line sources, subsurface cavity sources and furrows.

Acknowledgments This work was supported by The United States–Israel Binational Agricultural Research and Development fund (BARD), Project Grant Agreement No. US-3662-05R.

References

1. Bresler E (1978) Analysis of trickle irrigation with application to design problems. Irrig Sci 1:3–17. doi:10.1007/BF00269003
2. Lubana PPS, Narda NK (2001) Soil and water modeling: soil water dynamics under trickle emitters—a review. J Agric Eng Res 78:217–232. doi:10.1006/jaer.2000.0650
3. Mmolawa K, Or D (2000) Water and solute dynamics under a drip-irrigated crop: experiments and analytical model. Trans ASAE 43:1597–1608
4. Mmolawa K, Or D (2003) Experimental and numerical evaluation of analytical volume balance model for soil water dynamics under drip irrigation. Soil Sci Soc Am J 67:1657–1671
5. Ben-Gal A, Lazarovitch N et al (2004) Subsurface drip irrigation in gravel-filled cavities. Vadose Zone J 3:1407–1413
6. Skaggs TH, Trout T et al (2004) Comparison of HYDRUS-2D simulations of drip irrigation with experimental observations. J Irrig Drain Eng 130:304–310. doi:10.1061/(ASCE)0733-9437(2004)130:4(304)
7. Green WH, Ampt GA (1911) Studies on soil physics. Part 1. The flow of air and water through soils. J Agric Sci 4:1–24
8. Gardner WR (1958) Some steady state solutions of unsaturated moisture flow equations with application to evaporation from a water table. Soil Sci 85:228–232
9. Warrick AW, Lazarovitch N (2007) Infiltration from a strip source. Water Resour Res 43:W03420. doi:10.1029/2006WR004975
10. Mansell RS, Ma L et al (2002) Adaptive grid refinement in numerical models for water flow and chemical transport in soil: a review. Vadose Zone J 1:222–238
11. Schaap MG, Bouten W (1996) Modeling water retention curves of sandy soils using neural networks. Water Resour Res 32: 3033–3040. doi:10.1029/96WR02278
12. Schaap MG, Leij FJ et al (1998) Neural network analysis for hierarchical prediction of soil hydraulic properties. Soil Sci Soc Am J 62:847–855
13. Minasny B, McBratney AB (2002) The neuro-m method for fitting neural network parametric pedotransfer functions. Soil Sci Soc Am J 66:352–361
14. Minasny B, Hopmans JW et al (2004) Neural networks prediction of soil hydraulic functions from multi-step outflow data. Soil Sci Soc Am J 68:417–429
15. Schaap MG, Leij FJ et al (2001) ROSETTA: a computer program for estimating soil hydraulic parameters with hierarchical pedotransfer functions. J Hydrol (Amst) 251:163–176. doi:10.1016/S0022-1694(01)00466-8
16. Schmitz GH, Schutze N et al (2002) New strategy for optimizing water application under drip irrigation. J Irrig Drain Eng 128: 287–297. doi:10.1061/(ASCE)0733-9437(2002)128:5(287)
17. Jiusheng L, Yoder RE et al (2004) Simulation of nitrate distribution under drip irrigation using artificial neural networks. Irrig Sci 23:29–37. doi:10.1007/s00271-003-0090-6
18. Richards LA (1931) Capillary conduction of liquids in porous mediums. Physics 1:318–333. doi:10.1063/1.1745010
19. Šimůnek J, Sejna M et al (1999) The HYDRUS-2D software package for simulating the two-dimensional movement of water, heat, and multiple solutes in variably-saturated media, version 2.0. US Salinity Laboratory, Riverside, CA
20. Lazarovitch N, Šimůnek J et al (2005) System-dependent boundary condition for water flow from subsurface source. Soil Sci Soc Am J 69:46–50
21. Gardenas AI, Hopmans JW et al (2005) Two-dimensional modeling of nitrate leaching for various fertigation scenarios under micro-irrigation. Agric Water Manag 74:21–242. doi:10.1016/j.agat.2004.11.011
22. Lazarovitch N, Warrick AW et al (2007) Water content distribution in drip irrigation described by moment analyses. Vadose Zone J 6:116–123. doi:10.2136/vzj2006.0052
23. Mualem Y (1976) A new model for predicting the hydraulic conductivity of unsaturated porous media. Water Resour Res 12: 513–522. doi:10.1029/WR012i003p00513
24. van Genuchten MT (1980) A closed-form equation for predicting the hydraulic conductivity of unsaturated soils. Soil Sci Soc Am J 44:892–898
25. Carsel RF, Parrish RS (1988) Developing joint probability distributions of soil water retention characteristics. Water Resour Res 24:755–769. doi:10.1029/WR024i005p00755
26. Poulton M (ed) (2001) Computational neural networks for geophysical data processing. Pergamon, Amsterdam
27. Hertz J, Krogh A et al (1991) Introduction to the theory of neural computation. Addison Wesley, New York
28. Bishop C (1995) Neural networks for pattern recognition. Oxford Press, London
29. StatSoft (2001) STATISTICA for Windows v. 6.0. StatSoft, Tulsa, OK